Inorganic Chemistry

Article

pubs.acs.org/IC

Hydrothermal Growth of Lanthanide Borosilicates: A Useful Approach to New Acentric Crystals Including a Derivative of Cappelenite

Carla C. Heyward, Colin D. McMillen, and Joseph W. Kolis*

Department of Chemistry and Center for Optical Materials Science and Engineering Technologies (COMSET), Clemson University, Clemson, South Carolina 29634, United States

Supporting Information

ABSTRACT: The reaction of barium borosilicate glasses in hydrothermal fluids with NaOH mineralizer at ca. 600−650 °C in the presence of various sources of Eu^{3+} ions leads to a new series of noncentrosymmetric single crystals characterized by single-crystal X-ray diffraction. Under three slightly different reaction modifications, three new Eu^{3+}-containing noncentrosymmetric single crystals were isolated and characterized. Using a barium borosolicate glass with Eu_2O_3 added to the reaction mixture led to $NaBaEuSi_3O_9$ (**1**), which crystallizes in the noncentrosymmetric orthorhombic space group $P2_12_12_1$ with unit cell parameters a = 5.6373(11) Å, b = 11.483(2) Å, and c = 12.535(2) Å and consists of Eu^{3+} ions linked by $Si_3O_9^{6-}$ rings. Using a similar glass feedstock with Eu^{3+} included in the starting glass composition led to the compound $NaBa_3Eu_3Si_6O_{20}$ (**2**), which was determined in the noncentrosymmetric polar space group *Ama*2 with unit cell parameters a = 14.777(3) Å, b = 23.926(5) Å, and c = 5.5533(11) Å. It is constructed of individual islands of $Si_4O_{13}^{10-}$ and lone $Si_2O_7^{6-}$ building fragments. Finally, use of the Eu-containing glass along with additional Eu_2O_3 led to the compound $BaEu_6(Si_3B_6O_{24})(OH)_2$ (**3**), which crystallizes in the polar space group *P6mm* with a = 10.8074(15) Å and c = 4.7296(9) Å. It is related to the rare and poorly understood mineral cappelenite $Ba(Y,RE)_6(Si_3B_6O_{24})F_2$ and contains six-membered tetrahedral borate rings linked by silicate tetrahedra. The high percentage of noncentrosymmetric crystals obtained from of a simple borosilicate glass starting material, along with various straightforward chemical additives, suggests strongly that many more noncentrosymmetric crystals can be isolated from this general system.

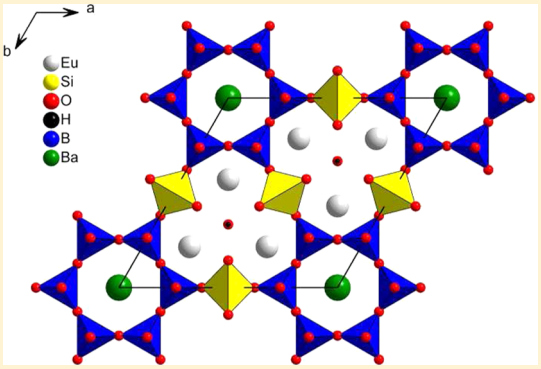

1. INTRODUCTION

The lack of a center of symmetry in a solid is the opening requirement in providing access to many new physical properties, including piezoelectricity, ferroelectricity, pyroelectricity, nonlinear optics, and a host of other interesting and useful effects.[1−5] Unfortunately, despite a considerable number of clever and dedicated efforts, it is not easy to rationally design acentric crystals.[6−10] Thus, the primary tactic is still exploratory synthesis. As stated succinctly, "First Comes the Synthesis",[11] and that is still the principal tool in finding new acentric inorganic crystals. In order to maximize the chances of success, it is beneficial to investigate systems that provide the highest probability of acentric crystal growth. One system that provides a reasonably high statistically favorable distribution of acentric structures is metal borates.[12] This class of compounds generates, on average, over 30% acentric single-crystal structures, which is substantially greater than the whole pool of acentric inorganic single crystals (ca. 10% acentric).[13−15] The borates have another significant attractive quality as well in that they often have very wide transparent windows with band edges deep in the UV, sometimes below 170 nm.[12] This makes them very appealing for very short-wavelength nonlinear-optical (NLO) applications like deep-UV solid-state lasers.[16]

Unfortunately, the demands for such deep-UV laser applications are so stringent that the pool of successful candidates is very small. If one is willing to sacrifice some width in the band edge and allow the band edge to move somewhat above 200 nm, a much greater palette of compounds can be addressed. Recently, metal borosilicates and borogermanates have been capturing attention as both interesting structural materials and acentric crystalline materials. For example, the stillwellite derivatives, $REBSiO_5$ and $REBGeO_5$, display good NLO properties and even suggest that they can be periodically poled, which could greatly enhance their performance parameters.[17−19]

A recent review of the borogermanates gives just a hint of the vast structural and chemical variety available to the field as well as the diverse solid-state chemistry that awaits.[20] Perhaps, most

Special Issue: To Honor the Memory of Prof. John D. Corbett

Received: September 18, 2014
Published: November 25, 2014

   dx.doi.org/10.1021/ic502279n | Inorg. Chem. 2015, 54, 905−913

importantly, an examination of the borogermanate crystals listed in that manuscript shows that, of the 20 strictly inorganic crystals listed in the review, 13 are acentric. This is one of the highest percentages of any field and suggests that this particular category can be a rich hunting ground for new acentric crystals.

Metal borosilicates should present some chemistry analogous to that of borogermanates but may have some significant differences as well. Germanates display a wider range of coordination environments around the Ge centers, including tetrahedral, trigonal-bipyramidal, and octahedral coordination, versus the silicates, which should almost exclusively adopt tetrahedral coordination around the Si atoms. Borates adopt either trigonal-planar or tetrahedral environments that, like in the polysilicates, can form an enormous variety of rings and chains.[21] In the case of borosilicates, all of these various building blocks can mix and match to form polynuclear rings and chains with an infinite variety of structural possibilities. Because silicate is harder and less polarizable than the germanate analogues, its presence in the building blocks may provide a slightly wider window with a shorter-wavelength band edge. The enormous structural diversity and the potential for growing acentric single crystals certainly make the borosilicate class worth exploring.

Our long-term hydrothermal crystal growth project led to an extensive array of alkaline-earth borate and silicate single crystals.[22,23] Recently, we started to investigate the doping of Eu^{2+} into a variety of barium borosilicates to study their potential as phosphors, especially in apatite phases.[24,25] In the course of these studies, we also discovered that, under the appropriate conditions, we can also prepare a number of new borosilicates wherein Eu^{3+} is also a major metal building block. The synthetic method is very simple and has the promise of enormous exploratory breadth. We find that even the simplest borosilicate glasses serve as an excellent source of feedstock for new europium borosilicate phases, a very high percentage of which are acentric.

In this paper, we describe our initial results using a simple barium borosilicate glass melt as a starting material with various europium sources under typical hydrothermal conditions to prepare a series of new europium borosilicate crystals and their acentric structures. Three new structures have been identified, and all are acentric, suggesting that this is a high-percentage approach to new acentric crystals. The high-temperature hydrothermal method has proven to be extremely useful in the growth of high-quality oxide- and fluoride-based single crystals for optical applications.[26] The presence of an Eu ion as a building block in the lattices suggests that other comparable lanthanides can be included, particularly spectrally silent host ions like Y^{3+} and Gd^{3+}. If they can serve as the metal building block, they can presumably be doped by lasing ions such as Nd^{3+} or Yb^{3+} to form self-frequency-doubling lasing crystals. In this intriguing class of solids, both lasing and second harmonic generation occur within the same crystal, which can be a very useful and interesting physical phenomenon.[27] Given the vast array of chemical variations of possible borosilicate glasses, the enormous number of potential combinations of borosilicate building blocks, and our high percentage of initial success in preparing acentric single crystals, we think that we have identified a path to a massive list of new acentric metal borosilicate single crystals.

2. EXPERIMENTAL METHODS

2.1. Preparation of the Borosilicate Glass Starting Material. The borosilicate glasses are routinely prepared by simple melt methods. A typical precursor, barium borosilicate glass ("BaSiBO") starting material, was prepared by heating simple component oxides in platinum crucibles in air at 950 °C for 18 h using reaction formulas as follows: 2.5 g (36 mmol) of B_2O_3 (Alfa Aesar 98%), 0.72 g (12 mmol) of SiO_2 (Alfa Aesar 99.9%), and 1.84 g (12 mmol) of BaO (Alfa Aesar 99.5%), producing an opaque glassy material. The resultant glass was ground using a mortar and pestle to form a colorless powder that can be used as a feedstock in susbsequent hydrothermal growth reactions. The Eu-doped glass ("Eu:BaSiBO") can be prepared in a similar fashion by including 2.11 g (6 mmol) of Eu_2O_3 (Alfa Aesar 98%) with the other component oxides as above.

2.2. Hydrothermal Crystal Growth Technique. For the hydrothermal reactions, the powdered glass feedstock from above (along with an additional europium source, if desired) was weighed in a 2.5-in.-long silver tube with $^3/_8$ in. o.d. that had one end welded closed. The desired aqueous hydroxide mineralizer solution (see below) was added to a fill volume of approximately 60% of the remaining free volume, and the tube was then welded completely closed. The resultant sealed ampules were placed in a high-temperature autoclave that was then filled with water to an approximately similar degree of fill of the ampules, and the autoclave was heated to the desired temperature.[26] After the reaction period, the autoclave was cooled to room temperature, and the resultant crystals were harvested from the silver ampules.

2.3. Synthesis of $NaBaEuSi_3O_9$ (1). A feedstock material (0.3 g), "BaSiBO", was added to a $^3/_8$-in.-o.d, 2.5-in.-long ampule along with 0.24 g of Eu_2O_3 and 1.2 mL of 3 M NaOH. After it was welded shut, the tube was heated for 6 days at 620 °C under 1.5 kbar of pressure. The resulting products were a 50:50 mixture of a colorless powder and colorless rods. Using single-crystal X-ray diffraction (XRD), the colorless rods were determined to be **1**, crystallizing in the noncentrosymmetric orthorhombic space group $P2_12_12_1$. Elemental analysis by energy-dispersive X-ray supports the structure determination in terms of the relative ratios of the metals, with atomic percentages of O (67%), Si (14%), Na (5.5%), Ba (5.5%), and Eu (7.6%) (expected: 60% O, 20% Si, 6.7% Na, 6.7% Ba, and 6.7% Eu). Through the use of powder XRD, the resultant colorless powder in this reaction was found to be in good agreement with the pattern of the mineral spencite, an analogue in the apatite family having the formula $Eu_5(Si_2BO_{12})O$.[28] Steadily increasing the reaction temperature and concentration of the mineralizer to 640 °C and 5 M, respectively, produced increasingly more crystals of **1** than the previous reactions, but the reaction was never truly phase pure. The powder XRD pattern of the needles was found to match the calculated pattern from **1** (Supporting Information, Figure S1).

2.4. Synthesis of $NaBa_3Eu_3Si_6O_{20}$ (2). The feedstock material "Eu:BaSiBO" (0.3 g) was added to a $^3/_8$-in.-o.d, 2.5-in.-long ampule along with 1.2 mL of 1 M NaOH. After it was welded shut, the tube was heated for 6 days at 630 °C at 1.5 kbar of pressure. The resulting product was a series of colorless needles in high yield. A representative needle was characterized structurally as **2** by single-crystal XRD. Powder XRD of the composite reaction product indicated that the reaction was phase-pure because all peaks are accounted for by the simulated pattern of **2** from the single-crystal structure refinement (Supporting Information, Figure S2). Elemental analysis again indicates agreement in the relative ratios of the metals, with atomic percentages of O (60.6%), Si (17.9%), Na (3.1%), Ba (9.5%), and Eu (9.0%) (expected: 60.6% O, 18.2% Si, 3.0% Na, 9.1% Ba, and 9.1% Eu).

2.5. Synthesis of $BaEu_6(Si_3B_6O_{24})(OH)_2$ (3). The feedstock material "Eu:BaSiBO" (0.3 g) was added to a $^3/_8$-in.-o.d, 2.5-in.-long ampule along with 0.24 g of Eu_2O_3 and 1.2 mL of 3 M NaOH. After it was welded shut, the tube was heated for 6 days at 650 °C at 1.5 kbar of pressure. The resulting product was a mixture of a majority of colorless needles and a minority of colorless hexagonal plates and colorless microcrystalline powder. The hexagonal plates were found to

dx.doi.org/10.1021/ic502279n | Inorg. Chem. 2015, 54, 905−913

be **3** by single-crystal XRD. Powder XRD showed that the microcrystalline powder is a mixture of **3** and $EuBO_3$ (Supporting Information, Figure S3) and that the needlelike crystals are $Ba_3B_6O_{11}(OH)_2$.[29]

2.6. XRD. Single-crystal X-ray intensity data from compounds **1**–**3** were collected at room temperature using a Mercury charge-coupled detector and a Rigaku AFC8S diffractometer with graphite-monochromated Mo Kα radiation (λ = 0.71073 Å). All crystals diffracted strongly and required only 5 s of exposure over 480 diffraction images. This resulted in 7069 reflections (1479 unique) for **1**, 8953 reflections (1921 unique) for **2**, and 4235 reflections (377 unique) for **3**. Data were processed and corrected for absorption, Lorentz, and polarization effects using the *CrystalClear* software suite.[30] The structures were solved by direct methods and subsequently refined by full-matrix least squares on F^2 using the *SHELXTL* software suite.[31] All non-H atoms were refined anisotropically for all structures. In the case of **3**, the H atom attached to O5 was first identified from the difference map and then restrained as a riding atom on this O atom to maintain a reasonable distance during subsequent refinements. The resulting crystallographic data for **1**–**3** are shown in Table 1, and selected bond distances and angles are summarized in Table 2. In all cases, the systematic absences and intensity statistics were suggestive of noncentrosymmetric space groups, and the respective structures were solved in $P2_12_12_1$ for **1**, *Ama*2 for **2**, and *P*6*mm* for **3**. To better determine the absolute structures of these noncentrosymmetric materials, Friedel opposites were not merged at any point. For **2** and **3**, the resulting Flack parameters were found to be very close to 0, statistically suggesting the correct absolute structure. The structure of **1** was refined as a racemic twin, with a resulting BASF parameter of 0.40. To support the acentric structure of **1**, that structure was also determined in space group *P*1 and subjected to the *ADDSYM* analysis of the *PLATON* software package,[32] which confirmed the initial structure determination made in space group $P2_12_12_1$. Compounds **2** and **3** were also subjected to higher-symmetry searches, with no additional symmetry identified. A test refinement of **3** in space group *P*3 was also performed and is discussed in detail below. Powder XRD was also used to identify the reaction products, as well as confirm the structure determinations, by comparisons to data simulated from the final refinements (Supporting Information). Powder XRD analysis was performed using a Rigaku Ultima IV powder diffractometer with Cu Kα radiation (λ = 1.54056 Å). Data were collected in 0.02° steps from 2θ = 6 to 65° at a rate of 1°/min.

Table 1. Crystallographic Data for Compounds 1–3

	1	2	3
chemical formula	$NaBaEuSi_3O_9$	$NaBa_3Eu_3Si_6O_{20}$	$BaEu_6(Si_3B_6O_{24})(OH)_2$
fw (g/mol)	540.56	1379.43	1616.25
temperature (K)	293	293	293
cryst syst	orthorhombic	orthorhombic	hexagonal
space group	$P2_12_12_1$ (No. 19)	*Ama*2 (No. 40)	*P*6*mm* (No. 183)
unit cell dimens			
a (Å)	5.6373(11)	14.777(3)	10.8074(15)
b (Å)	11.483(2)	23.926(5)	10.8074(15)
c (Å)	12.535(3)	5.5533(11)	4.7296(9)
volume (Å^3)	811.4(3)	1963.4(7)	478.41(13)
Z	4	4	1
density (calcd) (g/cm^3)	4.425	4.667	5.610
μ (mm^{-1})	13.009	15.845	21.711
F(000)	976	2448	716
cryst size (mm^3)	0.41 × 0.12 × 0.11	0.44 × 0.09 × 0.07	0.20 × 0.20 × 0.07
2θ range (deg)	2.41–25.25	2.76–26.01	2.18–25.33
min, max indices	[−6, −13, −15], [6, 13, 15]	[−18, −29, −6], [18, 29, 6]	[−12, −13, −5], [13, 13, 5]
no. of reflns collcd	7069	8953	4235
no. of indep reflns	1479 [R_{int} = 0.0587]	1921 [R_{int} = 0.0671]	377 [R_{int} = 0.0789]
obsd reflns [$I > 2\sigma(I)$]	1368	1866	376
no. of param	137	163	48
final *R* [$I > 2\sigma(I)$]			
R1	0.0320	0.0285	0.0331
wR2	0.0668	0.0613	0.0807
final *R* (all data)			
R1	0.0369	0.0298	0.0332
wR2	0.0696	0.0618	0.0807
GOF (S)	1.198	1.135	1.189
extinction coeff		0.0007	0.0050
Flack parameter	0.40(3) (twin)	−0.06(2)	0.04(6)

3. RESULTS AND DISCUSSION

3.1. Synthetic Chemistry. Our original motivation in this study was the investigation of Eu^{2+}-doped barium borates and barium borosilicate crystals as a europium phosphor in apatites and related phases.[33] This seemingly simple investigation led to a complex interplay between Eu^{2+} and Eu^{3+} oxidation states, as well as the occasional incorporation of an Eu ion as a true building block rather than simple doping at the Ba site, leading to new europium silicates and borosilicates. These doping, redox, and emission studies are ongoing work done in parallel. Some of the materials that contained Eu as a building block in the structure caught our attention for other reasons, namely, their interesting solid-state structures (compounds **1**–**3** herein). All of the compounds in the present study possess trivalent Eu as a structural building block. For all of the reactions in this paper, we first prepared either a borosilicate glass using BaO as a glass fluxing agent to form a barium borosilicate ("BaBSiO") or an analogous borosilicate that also contains Eu ions included in the glass ("EuBaBSiO") in stoichiometric ratios equal to that of the Ba and silicate ions. This glass feedstock was then subjected to relatively high-temperature (ca. 600 °C) hydrothermal fluids in welded silver tubes. This approach added additional variety to the stoichiometric phase space by (1) the ability to enrich the reaction in Eu using additional Eu_2O_3 and 2) the use of mineralizer ions to facilitate crystal growth or participate in the reactions. Indeed, both the enrichment of the reaction with Eu and the presence of Na ions in the reaction proved critical in these syntheses.

For compound **1**, the reaction of the simple barium borosilicate glass with Eu_2O_3 in sodium hydroxide (approximate reaction stoichiometry of Ba:Eu:Na = 1:2:5) leads to an approximately equal mixture of a novel apatite phase $Eu_5(Si_2BO_{12})O$, which is analogous to the mineral spencite[28] and **1**. Of course, the apatite family is huge with many structural and chemical variations.[34] As such, it represents an example of an "adaptable solid structure".[35] In the case herein, the Eu ions are all in the trivalent state and the borosilicate ratio adapts for the appropriate charge balance. The apatite chemistry in this series of compounds is both subtle and complex and will be discussed in much greater detail in an upcoming publication. Various attempts to vary the mineralizer concentration,

dx.doi.org/10.1021/ic502279n | *Inorg. Chem.* 2015, 54, 905–913

Table 2. Selected Interatomic Distances (Å) and Angles (deg)

1		2		3	
Distances		Distances		Distances	
Eu1−O9	2.230(8)	Eu1−O6	2.272(6)	Eu1−O4 (×2)	2.360(6)
Eu1−O8	2.319(8)	Eu1−O3	2.320(8)	Eu1−O3 (×2)	2.362(5)
Eu1−O5	2.332(8)	Eu1−O10	2.328(6)	Eu1−O1	2.388(12)
Eu1−O1	2.346(8)	Eu1−O4	2.370(7)	Eu1−O5	2.454(8)
Eu1−O2	2.347(8)	Eu1−O2	2.446(6)	Eu1−O2 (×2)	2.636(8)
Eu1−O7	2.379(8)	Eu1−O9	2.452(7)		
		Eu1−O11	2.533(7)	Ba1−O1 (×6)	2.967(12)
Ba1−O9	2.691(8)	Eu2−O4 (×2)	2.279(6)	Ba1−O3 (×6)	2.991(11)
Ba1−O1	2.738(8)	Eu2−O11 (×2)	2.419(7)		
Ba1−O2	2.742(8)	Eu2−O9 (×2)	2.450(7)	Si1−O4 (×2)	1.610(10)
Ba1−O8	2.760(8)	Eu2−O10 (×2)	2.715(8)	Si1−O2 (×2)	1.673(11)
Ba1−O1	2.866(8)				
Ba1−O7	2.907(8)	Ba1−O7	2.648(10)	B1−O3	1.42(2)
Ba1−O5	2.940(8)	Ba1−O9 (×2)	2.727(7)	B1−O1 (×2)	1.461 (11)
Ba1−O2	3.007(9)	Ba1−O11 (×2)	2.805(7)	B1−O2	1.557(19)
		Ba1−O6 (×2)	2.855(7)		
Na1−O8	2.357(9)	Ba2−O2	2.610(7)	Angles	
Na1−O6	2.384(9)	Ba2−O2	2.745(8)	O2−Si1−O2	102.4(8)
Na1−O5	2.428(10)	Ba2−O12	2.770(7)	O2−Si1−O4	110.3(3)
Na1−O6	2.658(11)	Ba2−O3	2.821(8)	O4−Si1−O4	112.8(8)
Na1−O3	2.682(11)	Ba2−O6	2.887(7)		
Na1−O4	2.841(10)	Ba2−O3	2.904(8)	O1−B1−O1	108.4(4)
Na1−O7	2.884(11)	Ba2−O7	2.912(8)	O1−B1−O2	103.4(3)
		Ba2−O5	2.982(8)	O1−B1−O3	114.7(8)
Si1−O1	1.588(9)			O2−B1−O3	111.1(8)
Si1−O2	1.599(9)	Na1−O12	2.408(12)		
Si1−O3	1.665(8)	Na1−O8	2.410(10)	$[Si_3B_6O_{24}]$ Bridging Angles	
Si1−O4	1.675(8)	Na1−O1 (×2)	2.472(9)	B1−O2−Si1	115.1(6)
Si2−O7	1.591(8)	Na1−O10 (×2)	2.745(8)	B1−O1−B1	135.3(8)
Si2−O5	1.610(9)				
Si2−O4	1.664(9)	Si1−O3	1.605(8)		
Si2−O6	1.672(8)	Si1−O4	1.610(6)		
Si3−O9	1.588(8)	Si1−O1	1.639(7)		
Si3−O8	1.598(9)	Si1−O2	1.640(7)		
Si3−O3	1.644(9)	Si2−O7	1.598(12)		
Si3−O6	1.686(7)	Si2−O6 (×2)	1.637(7)		
		Si2−O5	1.686(9)		
$[Si_3O_9]$ Bridging Angles		Si3−O10	1.603(6)		
Si1−O3−Si3	124.6(5)	Si3−O11	1.615(7)		
Si1−O4−Si2	126.5(5)	Si3−O9	1.633(7)		
Si2−O6−Si3	127.5(5)	Si3−O8	1.656(3)		
		Si4−O12	1.588(11)		
		Si4−O1 (×2)	1.627(7)		
		Si4−O5	1.632(9)		
		$[Si_4O_{13}]$ Bridging Angles			
		Si1−O1−Si4	133.8(5)		
		Si2−O5−Si4	140.4(8)		
		$[Si_2O_7]$ Bridging Angle			
		Si3−O8−Si3	158.6(6)		

temperature, and reaction time did not significantly alter the final product ratio. In the case of product **1**, the alkali ion from the mineralizer became incorporated in **1**, but no borate from the glass was incorporated because that component appears to be segregated in the apatite product.

Different chemistry was observed when Eu was instead integrated into the borosilicate glass feedstock, resulting in the formation of **2** when the glass was subjected to the aqueous NaOH under hydrothermal conditions (approximate reaction stoichiometry of Ba:Eu:Na = 1:1:2.4). Interestingly, the initial stoichiometry of Ba:Eu in the glass appears to have been retained in the resulting product **2**, which formed as colorless rods in a phase-pure yield. In this case also, not only was the NaOH mineralizer able to induce crystallization, but the sodium ions also became part of the lattice of the final product. It is also worth noting that the relative amount of Na compared to Ba + Eu in the resulting product here is considerably less (1:6) than that in **1** (1:2). These ratios correspond to the lower

dx.doi.org/10.1021/ic502279n | *Inorg. Chem.* 2015, 54, 905−913

concentration of NaOH (1 M) used in the synthesis of **2** compared to that used to prepare **1** (3 M) and suggests further phase space may be easily accessed by simply varying the mineralizer concentrations. As with **1**, both Na and Ba ions are part of the building block units in the lattice along with the Eu^{3+} ions, but no B atoms are part of the construct, apparently instead forming a soluble species.

If the same Eu-doped glass is used under essentially identical reaction conditions but additional Eu_2O_3 is included in the initial hydrothermal reaction mixture (approximate reaction stoichiometry of Ba:Eu:Na = 1:3.8:7.2), then another acentric crystalline product is formed as a colorless powder and hexagonal plates of **3**. In this case, both B and Si atoms from the glass feedstock form part of the lattice along with the Eu^{3+} ions, whereas Na is absent. In keeping with the presence of increased Eu ions in the starting materials, the final product is fairly rich in Eu, having a Ba:Eu ratio of 1:6 compared to 1:1 in **1** and **2**. The crystal that forms is similar to the natural mineral cappelenite, which forms in the polar acentric space group $P3$.[36] The cappelenite phase is an extremely rare and very poorly understood mineral. Only a few examples are known in the world, and they are generally of very low crystalline quality and as such their characterization is limited. A single-crystal structure has been reported but required a rather elegant heat treatment of the mineral to induce crystal growth of a small fragment from the metamict natural state.[36] The end-member formula for cappelenite is reported as $BaY_6(Si_3B_6O_{24})F_2$, and the natural sample was found to contain additional K, Na, Ca, La, Th, and Ce.[37] The ability to grow high-quality single crystals of this structure type is exciting for a number of reasons. In addition to its attractive structural model, it is both acentric and polar, so it can be used for NLO as well as possibly for ferroic applications. If the lanthanide site can be properly doped and induced to act as a laser, then the acentric crystal can also act as a self-frequency-doubling laser. An investigation into the structure of a pure, synthetic end-member composition will also add to understanding this curious mineral. One approach we will investigate in the future will be the use of fluoride as the mineralizer in lieu of hydroxide to generate the natural fluoride analogue.

"BaSiBO" glass + Eu_2O_3 → $\underset{\mathbf{1}}{NaBaEuSi_3O_9}$

3 M NaOH/620 °C

"Eu: BaSiBO" glass → $\underset{\mathbf{2}}{NaBa_3Eu_3Si_6O_{20}}$

1 M NaOH/630 °C

"Eu: BaSiBO" glass + Eu_2O_3 → $\underset{\mathbf{3}}{BaEu_6(Si_3B_6O_{24})(OH)_2}$

3 M NaOH/650 °C

3.2. Crystal Structure of 1. Compound **1** crystallizes in the noncentrosymmetric orthorhombic space group $P2_12_12_1$ with unit cell parameters a = 5.6373(11) Å, b = 11.483(2) Å, and c = 12.535(2) Å. It appears to be the europium analogue of $NaBaNdSi_3O_9$ (a = 5.661 Å, b = 11.486 Å, and c = 12.591 Å), identified in 1984, during a preliminary investigation of potential laser materials in the Na_2O–BaO–Nd_2O_3–SiO_2–H_2O system.[38] This structure type is also reported to be shared by $NaBaNdGe_3O_9$,[39] but to our knowledge, there has been no follow-up work related to these compounds. The structure of **1** is a complex three-dimensional framework. The principal building block is a puckered $[Si_3O_9]$ cyclosilicate ring. The Si–O bond distances of the tetrahedra comprising the cyclosilicate range from 1.588(9) to 1.610(9) Å for bonds to the six terminal O atoms and from 1.644(9) to 1.686(7) Å for the three bridging O atoms. The O–Si–O bond angles range from 101.4(4) to 117.7(4)° within the cyclosilicate group. The isolated $[Si_3O_9]$ building blocks are connected through the Na, Eu, and Ba atoms to form the complex framework (Figure 1).

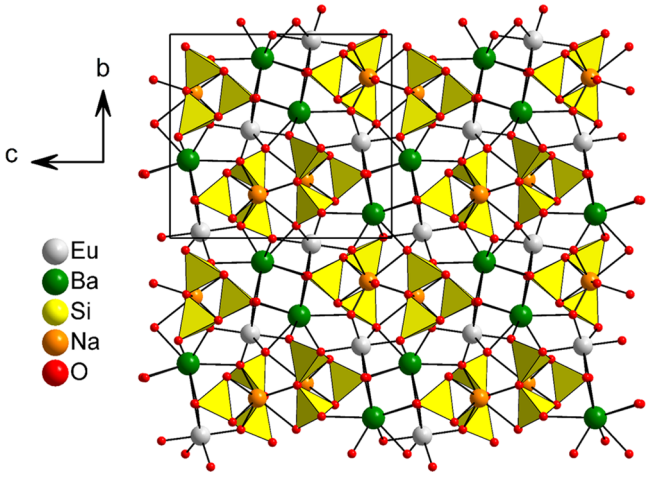

Figure 1. Framework structure of **1** based on the isolated $[Si_3O_9]$ cyclosilicate building block.

Bridging O atoms within the $[Si_3O_9]$ group connect only to Na atoms, while terminal O atoms can form bonds with all three metals. Na atoms are themselves in a distorted 7-coordinate environment with O, with Na–O bonds ranging from 2.357(9) to 2.884(10) Å. Through this connectivity, the Na atoms link to three $[Si_3O_9]$ rings (Figure 2a). Eu atoms are 6-coordinate with

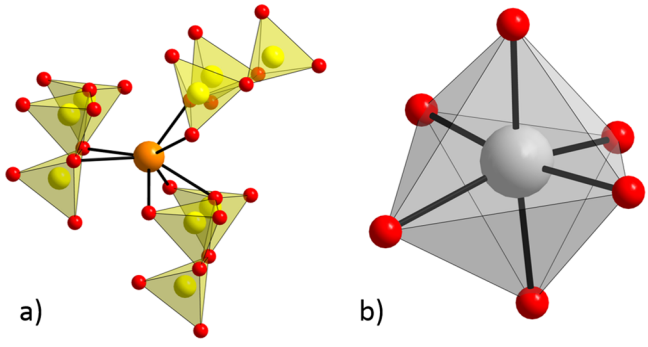

Figure 2. Selected coordination environments in **1**: (a) coordination about Na atoms; (b) coordination about Eu atoms.

O, forming a slightly distorted octahedron (Figure 2b). Here there is a fairly narrow range of Eu–O bond distances [2.300(8)–2.379(8) Å], and connectivity occurs to five $[Si_3O_9]$ groups. Ba is 8-coordinate with O, providing connections to six cyclosilicate units. Because Eu is intermediate in size among the lanthanides and the Eu site in **1** maintains a fairly narrow distribution of bond distances, it seems likely that analogous compounds based on both the larger and smaller lanthanides could also adopt this structure type under appropriate conditions. Crystal chemical substitution at the Na site may be more limited, however, because a mixture of fairly short and

dx.doi.org/10.1021/ic502279n | Inorg. Chem. 2015, 54, 905–913

fairly long interactions must be maintained to fit this structure type, making other structure types more likely for species based on other alkali metals.

3.3. Structure of 2. The structure of compound **2** was determined in the noncentrosymmetric polar space group *Ama*2 with unit cell parameters a = 14.777(3) Å, b = 23.926(5) Å, and c = 5.5533(11) Å. This compound appears to be analogous to a briefly reported compound $NaBa_3Nd_3Si_6O_{20}$ [space group *C*2*cm*, a = 5.590(2) Å, b = 24.136(6) Å, and c = 14.830(4) Å], but to our knowledge, there has been no follow-up work on this material or any related compounds.[40] The structure features two distinct, independent silicate arrangements as $[Si_4O_{13}]$ and $[Si_2O_7]$ groups, resulting in a structural formula of $NaBa_3Eu_3(Si_4O_{13})(Si_2O_7)$. The isolated $[Si_4O_{13}]$ group is an interesting and rather unusual building block among the silicates because this formulation most often occurs as finite chains.[41] As shown in Figure 3, the $[Si_4O_{13}]$ group in **2** occurs

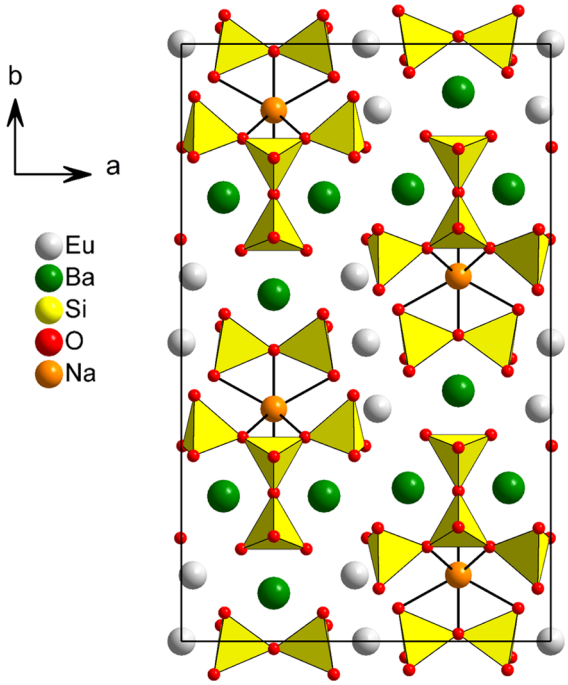

Figure 3. Unit cell of **2**, featuring isolated $[Si_4O_{13}]$ and $[Si_2O_7]$ building blocks.

as an isolated island, having mirror symmetry as a unit (or alternatively described as a branched $[Si_3O_{10}]$ chain in [41]). Here, the 3-fold axes of two of the silicate tetrahedra are aligned with the c axis, and the apical O atoms of these two tetrahedra point in the same direction, common to all of the $[Si_4O_{13}]$ units in the polar structure. The remaining silicate group occurs in the form of the common isolated $[Si_2O_7]$ pyrosilicate arrangement. Both silicate groups exhibit identical mean Si–O bond distances of 1.627(11) Å, although it should be noted that the aforementioned apical Si–O bonds of the $[Si_4O_{13}]$ group are slightly shorter [1.588(11) and 1.599(11) Å] than this average.

The silicate building blocks are linked by the Ba, Eu, and Na atoms to form a complex three-dimensional framework. The 6-coordinate Na atom is particularly interesting, adopting a distorted pentagonal-pyramidal geometry by sharing two edges with a single $[Si_2O_7]$ group, one edge with a $[Si_4O_{13}]$ group, and one corner with one of the apical O atoms of a second $[Si_4O_{13}]$ group (Figure 4a). This geometry results in some variety in the observed Na–O bond distances. Longer bonds

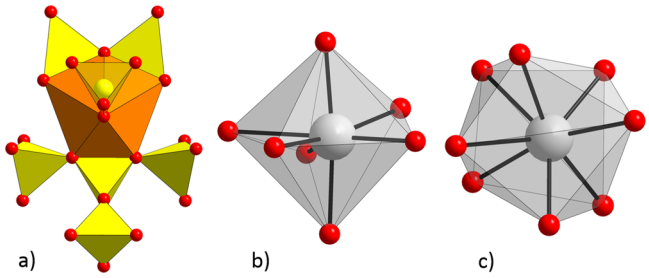

Figure 4. Selected coordination environments in **2**: (a) coordination of Na as a pentagonal pyramid between $[Si_4O_{13}]$ and $[Si_2O_7]$ groups (for clarity, only a portion of the $[Si_4O_{13}]$ group connecting to the apical O of the $[NaO_6]$ group is shown above the pyramid); (b) 7-coordinate Eu1; (c) 8-coordinate Eu2.

[2.745(8) Å] are formed with the terminal O atoms of the $[Si_2O_7]$ group, while shorter bonds are formed with the bridging O atom of the same group [2.410(10) Å] and bridging atoms of one $[Si_4O_{13}]$ group [2.472(9) Å]. The apical Na–O bond of the pentagonal pyramid, sharing the O atom with the apical bond of the $[Si_4O_{13}]$ group, is the shortest of all [2.408(12) Å], indicating a tight fit of the Na atoms between these silicate groups. Like **1**, this may limit the types of atoms that can be accommodated at this site for a limited variety of crystal chemistry. The Eu atoms (Figure 4b,c) are 7-coordinate (Eu1, pentagonal bypyramid) and 8-coordinate (Eu2, square antiprism), while the Ba atoms are also 7-coordinate (Ba1, trigonal prism) and 8-coordinate (Ba2, distorted cube).

3.4. Structure of 3. Compound **3** crystallizes in space group *P*6*mm* with a = 10.8074(15) Å and c = 4.7296(9) Å. It is related to the rare mineral cappelenite, $Ba(Y,RE)_6(Si_3B_6O_{24})F_2$, the structure of which was determined by Shen and Moore in 1984 [a = 10.67(2) Å and c = 4.680(2) Å].[36] Interestingly, their refinement on the naturally occurring sample was only successful in space group *P*3 because of distortion of the electron density about the Y sites in space groups *P*6*mm* and *P*3*m*1. In their study, segregation of Y into two independent sites in *P*3 led to good convergence and was attributed to the presence of the natural impurities in the mineral. In fact, they initially proposed that structural analysis on a pure sample may refine well in *P*6*mm*. Indeed, we note that the structure of our synthetic analogue can be solved to convergence in both *P*3 and *P*6*mm*. Refinement of our data in *P*6*mm* leads to improved residual values (R1 = 0.0331 vs 0.0362) for fewer parameters (48 vs 130) compared to the test case in *P*3. The use of *PLATON* to search for higher symmetry in the test refinement also recommended a transformation from *P*3 to *P*6*mm*. Given the rarity and poor crystalline quality of the mineral and the challenges encountered both in the preparation of the natural sample for analysis and in the actual structure determination, the hydrothermal method of the present study has proven quite useful to prepare the pure sample needed to verify this 30-year-old hypothesis. We note that the presence of fluoride in the few ill-characterized samples of natural cappelenite is somewhat ambiguous, and it is clearly not present in our reaction mixtures. We confirmed the presence of OH^- in the lattice of **3** by the characteristic absorption band from 3400 to 3500 cm^{-1} in the IR absorption analysis (Supporting Information, Figure S4). The present study, demonstrating that cappelenite-type

dx.doi.org/10.1021/ic502279n | *Inorg. Chem.* 2015, 54, 905–913

phases form readily in alkali basic hydrothermal fluids (a condition of which obviously also exists in many natural systems), would certainly support the ideas of substitution or mixed occupancy of OH^- and F^- in the natural sample, which could be the source of the uncertain F analyses in those studies.

The structure itself is an excellent example of acentric, polar building blocks assembling in a polar fashion. The basic framework for the structure is formed by tetrahedral borate and silicate building blocks. Six borate groups are connected by corner sharing to form $[B_6O_{18}]$ rings. These rings are connected to one another by B−O−Si−O−B corner sharing through the $[SiO_4]$ tetrahedra to form the overall $[Si_3B_6O_{24}]$ borosilicate sheet that extends infinitely in the *ab* plane (Figure 5). These sheets establish the polar nature of the structure

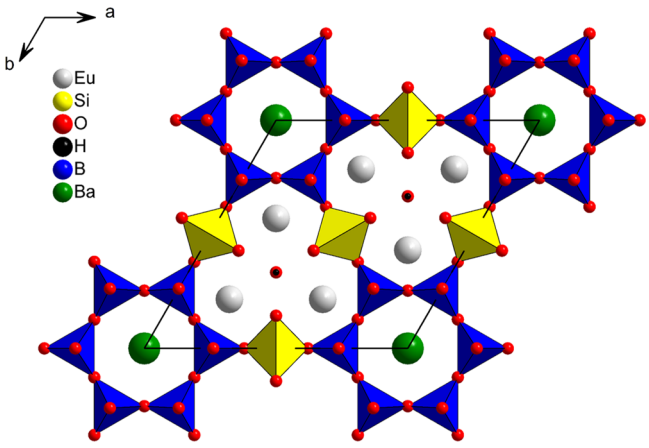

Figure 5. Structure of cappelenite-type **3** along [001]. This synthetic analogue exhibits the ideal *6mm* symmetry that is only approximately achieved in the natural mineral.

because there is a concerted directionality to the apical O atoms of the borate tetrahedra along the *c* axis. The sheets contain two types of channels: Ba atoms are aligned with the hexagonal channels bound by $[B_6O_{18}]$, and clusters of Eu atoms are aligned with the channels bound by $[Si_3B_6O_{27}]$. The Ba and Eu atoms thus form a layer of their own in the structure, alternating with the borosilicate sheet along the *c* axis (Figure 6). Ba atoms are 12-coordinate with O, and Eu atoms are 8-coordinate with O in the form of $[EuO_7(OH)]$. The Eu atoms can be thought of as forming clusters where three edge-sharing Eu atoms share the O atom of the OH group as a common μ_3 vertex (Figure 7). This O vertex is out of the plane with the Eu

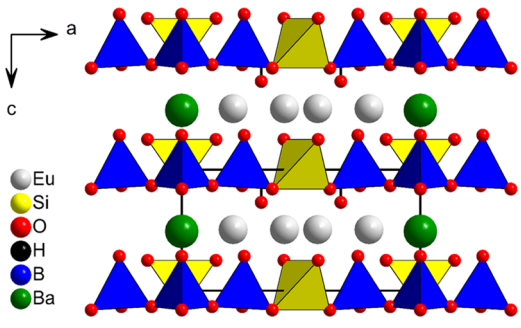

Figure 6. Alternating layers of borosilicate sheets with Ba and Eu atoms in **3**. Polarity is exhibited by the directionality of the apical O atoms of the $[BO_4]$ groups along [001].

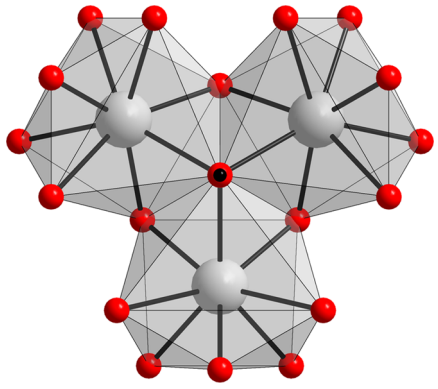

Figure 7. Edge-sharing clusters of $[EuO_7(OH)]$ along [001] in the ideal cappelenite structure.

atoms, and the O−H bond extends along the *c* axis, again exhibiting polar character in this direction. Two such clusters connect by shared O edges, accounting for the six Eu atoms and two OH groups in the unit cell.

As one may expect, there are some subtle differences in the structure of natural cappelenite in space group *P*3 and the "ideal" cappelenite-type structure of **3** in *P6mm*. We first note differences in the $[B_6O_{18}]$ group, which in cappelenite forms a distorted hexagonal channel but in **3** exhibits true 6-fold symmetry. Examining the individual borate tetrahedra, both structures have the same typical average B−O bond distance (1.475 Å) but seem to arrive there in different ways. Cappelenite exhibits unusually short apical B−O bonds (1.35 Å), with remaining B−O bonds of 1.50−1.55 Å within the $[B_6O_{18}]$ ring. The apical B−O3 bonds of **3** are still short (1.42(2) Å) but much closer to those exhibited by the bridging B−O1 bonds within the ring [1.461(11) Å]. This leads to only one longer than average B−O bond, B−O2 [1.557(19) Å], which bridges to the silicate group. Significant differences in the characteristics of the two unique Y sites in cappelenite, as noted by Shen and Moore, also contribute to its lower symmetry. Those two sites exhibit two slightly different average Y−O/F bond distances (2.38 and 2.43 Å) but quite different ranges (2.32−2.42 Å for Y1 and 2.23−2.75 Å for Y2). In **3**, there is one unique Eu site with a narrower range of the Eu−O bond distances ranging from 2.360(6) to 2.636(7) Å and averaging 2.445(12) Å. This is not simply an artifact of enforcing higher symmetry: the test refinement of **3** in *P*3 showed Eu1 to have bonds to O ranging from 2.351(7) to 2.622(8) Å and Eu2 to have bonds to O ranging from 2.351(7) to 2.659(8) Å. So, in the case of **3**, the sites remained effectively identical even with relaxed symmetry restrictions (Supporting Information, Table S1), whereas they are clearly unique in natural cappelenite. These two areas of distortion in natural cappelenite are somewhat dependent on one another because the shortest Y2−O bond and the two longest Y2−O bonds occur between O atoms that form the edges of borate tetrahedra. Similar effects are seen in the Ba coordination, with Ba−O bond distances ranging from 2.75 to 3.20 Å in natural cappelenite compared to 2.967(11)−2.991(11) Å in **3** (for the test refinement of **3** in *P*3, a similarly narrow range of 2.957(9)−2.995(9) Å was observed). The extremes of the Ba−O bond distances in natural cappelenite are again associated with the bridging O atoms in the distorted $[B_6O_{18}]$ ring. So, as the borate group "breathes" into true hexagonal symmetry in **3**, distortions in the Ba and rare-earth sites are relieved (or vice versa). Whether

dx.doi.org/10.1021/ic502279n | *Inorg. Chem.* 2015, 54, 905−913

material purity, lack of thermal reconstitution, or some other factor is the trigger for crystallization in the ideal hexagonal symmetry, the hydrothermal synthesis of this cappelenite analogue has proven to be a rewarding journey back into the mineralogical literature that holds future promise for the synthesis of polar inorganic solids.

4. CONCLUSIONS

This paper is a preliminary report of the hydrothermal growth of a series of Eu-containing silicate and borosilicate single crystals. Herein we identify a simple route to a potentially inexhaustible supply of new acentric, polar, lasing, and ferroic crystals. Three new materials were identified and structurally characterized in this initial work, all containing Eu^{3+} ions as key building blocks. All three feature noncentrosymmetric structures, with **1** crystallizing in the biaxial space group $P2_12_12_1$, **2** crystallizing in the polar biaxial space group *Ama*2, and **3** crystallizing in the uniaxial polar space group *P6mm* having structural similarity to the very rare mineral cappelenite. All of the materials are prepared straightforwardly from a simple premade glass, where the presence of an additional Eu source and Na ions from the mineralizer solution in the hydrothermal reaction play key roles in determining the outcome of the different phases. The very high percentage of acentric crystals isolated from these preliminary reactions is commensurate with the observation regarding the borogermanate phases, which also shows a very high percentage of acentric structure types. We are particularly excited about the potential of **3** as the prototype of a whole new family of important compounds. In addition to being acentric, the space group *P6mm* is polar and potentially ferroic, so an enormous array of physical properties may be accessed by the various members of this family. The presence of Eu^{3+} as a building block suggests strongly that most of the other lanthanides can be used in the lattices. Given that the original (only) cappelenite crystal reported is predominantly yttrium at the lanthanide site and that Eu^{3+} and Y^{3+} have quite similar ionic radii, we are hopeful that the yttrium analogue of **3** can likewise be prepared as high-quality crystals. If that is the case, then there is a very real chance that the Y^{3+} site can be doped with a lasing ion like Nd^{3+} or Yb^{3+} to create a series of self-frequency-doubling crystals. It is clear that this work is only in its earliest stages, with a great variety of experimental variables to be pursued in glass composition, mineralizer concentration, and lanthanide ions of interest. Interesting structural chemistry and unique physical properties continue to be the rewards of a synthesis-first approach.

■ ASSOCIATED CONTENT

Ⓢ Supporting Information

Powder XRD patterns for **1**−**3**, IR spectrum of **3**, bond valence comparison for the *P*3 and *P6mm* structures of **3**, and crystal structure data in CIF format. This material is available free of charge via the Internet at http://pubs.acs.org.

■ AUTHOR INFORMATION

Corresponding Author

*E-mail: kjoseph@clemson.edu.

Notes

The authors declare no competing financial interest.

■ ACKNOWLEDGMENTS

We are grateful to the National Science Foundation (Grants DMR-0907395 and DMR-1410727) for funding and support. In addition, J.W.K. acknowledges a debt to John Corbett, who, after presenting a memorable Saturday morning seminar on Zintl ions in 1981, encouraged the author to "always look in dark corners of the chemical attic".

■ REFERENCES

(1) Halasyamani, P. S.; Poeppelmeier, K. R. *Chem. Mater.* **1998**, *10*, 2753−2769.
(2) Bordui, P. F.; Fejer, M. M. *Annu. Rev. Mater. Sci.* **1993**, *23*, 321−379.
(3) Garmire, E. *Opt. Express* **2013**, *21*, 30532−30544.
(4) Abrahams, S. C. *Acta Crystallogr., Sect. A* **1994**, *A50*, 658−685.
(5) Laudise, R. A. *Bell Lab. Rec.* **1968**, *46* (January), 2−7.
(6) Halasyamani, P. S. *J. Solid State Chem.* **2012**, *195*, 1.
(7) Chen, C. T. *Annu. Rev. Mater. Sci.* **1986**, *16*, 203−243.
(8) Kunz, M. *J. Solid State Chem.* **1995**, *115*, 395−406.
(9) Gopalakrishnan, J.; Ramesha, K.; Rangan, K. K.; Panday, S. *J. Solid State Chem.* **1999**, *148*, 75−80.
(10) Chen, C. T.; Ye, N.; Lin, J.; Jiang, J.; Zeng, W.; Wu, B. *Adv. Mater.* **1999**, *11*, 1071−1078.
(11) Corbett, J. D. *Acc. Chem. Res.* **1981**, *14*, 239−246.
(12) Chen, C.; Sasaki, T.; Li, R.; Wu, Y.; Lin, Z.; Mori, Y.; Hu, Z.; Wang, J.; Aka, G.; Yoshimura, M.; Kaneda, Y. *Nonlinear Optical Borate Crystals: Principals and Applications*; Wiley-VCH: Weinheim, Germany, 2012.
(13) Chen, C.; Lin, Z.; Wang, Z. *Appl. Phys. B: Lasers Opt.* **2005**, *B80*, 1−25.
(14) Mori, Y.; Yap, Y. K.; Kamimura, T.; Yoshimura, M.; Sasaki, T. *Opt. Mater.* **2002**, *19*, 1−5.
(15) Becker, P. *Adv. Mater.* **1998**, *10*, 979−992.
(16) McMillen, C. D.; Kolis, J. W. *J. Cryst. Growth* **2008**, *310*, 2033−2038.
(17) Kaminskii, A.; Mill, B. V.; Butashin, A. V. *Phys. Status Solidi A* **1990**, *118*, K59.
(18) Chi, L.; Chen, H.; Zhuang, H.; Huang, J. *J. Alloys Compd.* **1997**, *252*, L12−L15.
(19) Sakaira, M.; Hirohashi, J.; Takekawa, S.; Miyazawa, S.; Furukawa, Y. *6th International Workshop on Crystallization*; Growth Technology: Somerset, U.K., 2013; Abstract P2.12.
(20) Zhang, J.-H.; Kong, F.; Xu, X.; Mao, J.-G. *J. Solid State Chem.* **2012**, *195*, 63−72.
(21) Grice, J. D.; Burns, P. C.; Hawthorne, M. F. *Can. Miner.* **1999**, *37*, 731−762.
(22) McMillen, C. D.; Stritzinger, J. T.; Kolis, J. W. *Inorg. Chem.* **2012**, *51*, 3953−3955 and references cited therein.
(23) McMillen, C. D.; Emirdag-Eanes, M.; Stritzinger, J. T.; Kolis, J. W. *J. Solid State Chem.* **2012**, *195*, 155−160.
(24) Heyward, C. C. Hydrothermal Crystal Growth of Metal Borates for Optical Applications. Ph.D. Dissertation, Clemson University, Clemson, SC, 2013.
(25) Heyward, C. C.; McMillen, C. D.; Kolis, J. W. Manuscript in preparation.
(26) McMillen, C. D.; Kolis, J. W. *Philos. Mag.* **2012**, *92*, 2686−2711.
(27) Jaque, D.; Capmany, J.; Sanz Garcia, J. A.; Brenier, A.; Boulon, G.; Garcia Sole, J. *Opt. Mater.* **1990**, *13*, 147−157.
(28) Jaffe, H. W.; Molenski, V. J. *Am. Mineral.* **1962**, *47*, 9−25.
(29) Heyward, C.; McMillen, C.; Kolis, J. W. *Inorg. Chem.* **2012**, *51*, 3956−3962.
(30) *CrystalClear*; Rigaku and Molecular Structure Corp.: The Woodlands, TX, 2006.
(31) Sheldrick, G. M. *Acta Crystallogr., Sect. A* **2008**, *A64*, 112−122.
(32) Spek, A. L. *J. Appl. Crystallogr.* **2003**, *36*, 7−13.
(33) Kottaisamy, M.; Jagannathant, R.; Jeyagopal, P.; Rao, R. P.; Narayanan, R. L. *J. Phys. D: Appl. Phys.* **1994**, *27*, 2210−2215.
(34) White, T. J.; Li, D. Z. *Acta Crystallogr., Sect. B* **2003**, *B59*, 1−16.

(35) Smit, J. P.; Stair, P. C.; Poeppelmeier, K. R. *Chem.—Eur. J.* **2006**, *12*, 5944−5953.
(36) Shen, J.; Moore, P. B. *Am. Mineral.* **1984**, *69*, 190−195.
(37) Brøgger, W. C. *Z. Kristallogr. Mineral.* **1890**, *16*, 462−467.
(38) Malinovskii, Y. A.; Bondareva, O. S.; Baturin, S. V. *Dokl. Akad. Nauk SSSR* **1984**, *275*, 372−375.
(39) Malinovskii, Y. A.; Belokoneva, E. L.; Demianets, L. N. *Zh. Strukt. Khim.* **1991**, *32*, 90−92.
(40) Malinovskii, Y. A.; Baturin, S. V.; Bondareva, O. S. *Dokl. Akad. Nauk SSSR* **1983**, *272*, 865−869.
(41) Wierzbicka-Wieczorek, M.; Kolitsch, U.; Tillmanns, E. *Acta Crystallogr., Sect. C* **2010**, *C66*, i29−i32 and references cited therein.